

Multimodal Nonlinear Optical Microscopy and Applications to Central Nervous System Imaging

Terry B. Huff, Yunzhou Shi, *Student Member, IEEE*, Yan Fu, Haifeng Wang, *Member, IEEE*, and Ji-Xin Cheng

(Invited Paper)

Abstract—Multimodal nonlinear optical (NLO) imaging is poised to become a powerful tool in bioimaging given its ability to capitalize on the unique advantages possessed by different NLO imaging modalities. The integration of different imaging modalities such as two-photon-excited fluorescence, sum frequency generation, and coherent anti-Stokes Raman scattering on the same platform can facilitate simultaneous imaging of different biological structures. Parameters to be considered in constructing a multimodal NLO microscope are discussed with emphasis on achieving a compromise in these parameters for efficient signal generation with each imaging modality. As an example of biomedical applications, multimodal NLO imaging is utilized to investigate the central nervous system in healthy and diseased states.

Index Terms—Central nervous system imaging, multimodality, nonlinear optical (NLO) microscopy.

I. INTRODUCTION

THE DEVELOPMENT of novel imaging technologies has opened new doors in our understanding of the nervous system in health and disease. For instance, electron microscopy (EM) has revealed the structure of the myelin sheath with unparalleled resolution [1]. Magnetic resonance imaging allows for the noninvasive study of lesion progression in neurological diseases such as multiple sclerosis [2] and confocal microscopy studies have revealed the dynamics of microglial cell activation in response to trauma in rat brain slices [3]. Despite the advances facilitated by these technologies, the limitations posed by them highlight the need for a more robust imaging method. Dehydration and staining in EM preclude its application for observing real-time processes. Magnetic resonance imaging lacks single-cell resolution. Confocal fluorescence is hindered both by low penetration depth limiting its applications for *in vivo* studies and by photobleaching that can complicate image acquisition and analysis.

Nonlinear optical (NLO) microscopy [4] is becoming a powerful tool for studying live tissues and live animals due to several

unique advantages over traditional methods. Nonlinear dependence on excitation intensity gives NLO microscopy inherent 3-D imaging capability without the need for a confocal pinhole. This is particularly advantageous in the case of tissue and *in vivo* imaging where significant scattering can reduce the signal collection efficiency by confocal detection. Laser scanning facilitates real-time imaging of live tissues and animals [5]. Also, NLO microscopy utilizes near-IR excitation that provides both superior optical penetration into tissues [6] as well as reduced photodamage due to reduced interaction with endogenous molecules [7]. Furthermore, different NLO imaging modalities are sensitive for probing different cellular structures.

In order to provide a robust imaging system, it is necessary to combine several NLO imaging modalities on the same platform. Multimodality in NLO imaging has been demonstrated to be a valuable tool for bioimaging. Fu *et al.* demonstrated simultaneous coherent anti-Stokes Raman scattering (CARS) imaging of axonal myelin and sum-frequency generation (SFG) imaging of astrocyte processes in live spinal tissues [8]. Nan *et al.* combined CARS with two-photon-excited fluorescence (TPEF) to investigate the relationship between mitochondria and lipid droplets in tumor cells [9]. Multimodality was also utilized to investigate the impact of obesity on tumor stroma [10] as well as to map atheroma in pig artery based on molecular composition [11].

In this paper, we systematically describe the integration of CARS, SFG, and TPEF microscopy. We discuss their unique advantages, the parameters to be considered in constructing a multimodal NLO microscope, and how to realize such a system. Finally, we show biomedical applications in that multimodal NLO microscopy was utilized to reveal the relationship between different structures in central nervous system and calcium ion influx into axons during demyelination, demonstrating its potential in addressing biological and biomedical questions.

II. MULTIMODAL NLO IMAGING

Fig. 1 shows an energy diagram of three NLO imaging methods that are most widely employed. They are briefly summarized as follows.

A. Two-Photon-Excited Fluorescence

In TPEF, the target molecule absorbs two photons to reach an excited electronic state and then emits a single-fluorescence photon of higher energy than either of the incident photons. Comparing with one-photon fluorescence, TPEF provides inherent 3-D resolution with tightly focused excitation. It also provides larger penetration depth due to the use of longer

Manuscript received October 1, 2007; revised November 14, 2007. This work was supported in part by the National Institutes of Health (NIH) under Grant R01 EB007243-01 and in part by the National Science Foundation (NSF) under Grant 0416785.

T. B. Huff is with the Department of Chemistry, Purdue University, West Lafayette, IN 47906 USA (e-mail: tbhuff@purdue.edu).

Y. Shi, Y. Fu, and H. Wang are with Weldon School of Biomedical Engineering, Purdue University, West Lafayette, IN 47906 USA (e-mail: shi5@purdue.edu; fuy@purdue.edu; wanghai@ecn.purdue.edu).

J.-X. Cheng is with the Department of Chemistry and Weldon School of Biomedical Engineering, Purdue University, West Lafayette, IN 47906 USA (e-mail: jcheng@purdue.edu).

Color versions of one or more of the figures in this paper are available online at <http://ieeexplore.ieee.org>.

Digital Object Identifier 10.1109/JSTQE.2007.913419

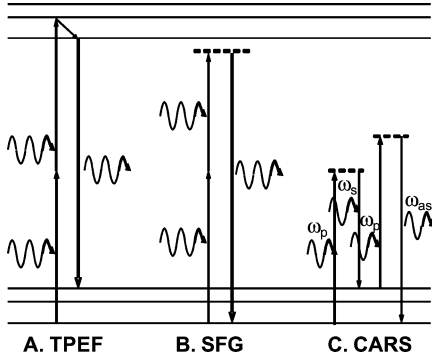


Fig. 1. Energy diagram. (A) TPEF. (B) SFG. (C) CARS.

wavelength excitations. TPEF is the most widely used NLO imaging modality owing to the wide availability of fluorescent labels and has become a potent tool for numerous studies in biology [12].

B. Sum-Frequency Generation

SFG is a second-order NLO process in which two incident photons are converted to one emission photon with energy exactly equal to the sum of the excitation photons [13]. SFG is selectively sensitive to noncentrosymmetric structures. Second harmonic generation (SHG) is a special case of SFG in which the two excitation photons are degenerate. SHG/SFG microscopy [14] has been demonstrated to be a sensitive probe of fibrous structures such as collagen [15] and astroglial processes [8].

C. Coherent Anti-Stokes Raman Scattering

CARS is a four-wave mixing process in which a pump beam (ω_p) and a Stokes beam (ω_s) interact with a sample to generate a signal at the anti-Stokes frequency $\omega_{as} = 2\omega_p - \omega_s$ (for reviews, see [16] and [17]). Because CARS signal can be significantly enhanced by molecular vibrations when $\omega_p - \omega_s$ is close to the vibrational frequency of a chemical bond, the CARS microscopy allows chemically selective imaging without fluorescence labeling. Furthermore, coherent addition of CARS emission from all molecules produces a large and directional CARS signal. CARS has been demonstrated to be a useful probe of lipid rich structures such as the myelin sheath in the nervous system [18].

With the aforementioned advantages, each imaging modality has its own drawbacks. TPEF can be complicated by inefficient or nonspecific dye labeling. Also, in order to distinguish between different structures and cells staining with multiple fluorophores is required [19]. SFG is insensitive to centrosymmetric structures limiting its application to molecular assemblies that lack inversion symmetry [13]. Lastly, CARS suffers from the presence of a nonresonant background that can overwhelm the resonant signal from weak Raman bands [16]. Thus, a more powerful microscopy system would facilitate the simultaneous application of multiple NLO imaging modalities in order to best take the advantage of the strengths of each method. As shown in Fig. 1, the same two laser beams that are used for CARS

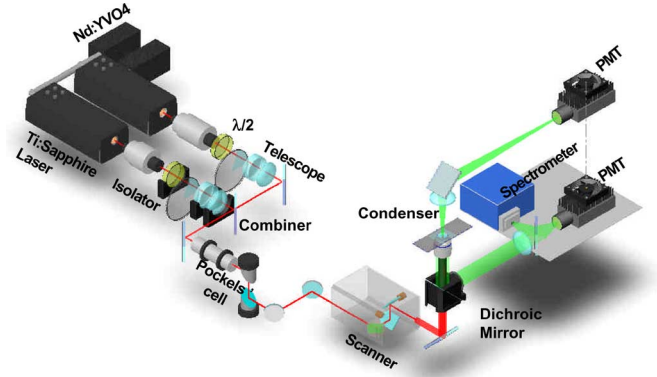


Fig. 2. Diagram of a multimodal NLO microscope. The two synchronized picosecond laser beams are collinearly combined, transmitted through a Pockels' cell, and directed into a laser-scanning microscope. For both beams, a half-wave plate is placed after the isolator to ensure horizontal laser polarization. The Pockels' cell is used to reduce the repetition rate of both lasers. The F-CARS signal is detected by a PMT installed after the condenser. The E-CARS, SFG, or TPEF signals can be detected by a PMT either externally in the nondescanned position or by internally housed PMTs in the descanned position.

imaging can also be used for the SFG imaging whereas either beam can be used for TPEF imaging. Therefore, the SFG and the TPEF modalities can be naturally integrated into a CARS microscope.

III. CONSTRUCTING A MULTIMODAL NLO MICROSCOPE

Our laboratory has developed multimodal NLO microscopy capable of simultaneous TPEF, SFG, and CARS imaging of the same sample. A typical setup built in our laboratory is shown in Fig. 2. To construct such a system, numerous parameters must be considered as the optimal conditions for signal generation in TPEF and SFG differ considerably from those for CARS imaging. We have approached the construction of a multimodal NLO microscope with emphasis on integrating TPEF and SFG imaging on a CARS microscope.

A. Excitation Sources

Although it is generally accepted that femtosecond pulses deliver the high peak power desirable for NLO imaging, Cheng *et al.* realized that this is not valid in the case of CARS microscopy [20]. The spectral profile of a femtosecond pulse is much broader than the typical Raman band ($8\text{--}10\text{ cm}^{-1}$); thus, the use of femtosecond pulses, which are preferred for TPEF and SFG, results in low spectral resolution in CARS microscopy. In the case of an isolated Raman band, only a fraction of the pulse energy is used to generate resonant signal with the rest only serving to increase the nonresonant background [20].

Pulses of a few picoseconds, on the other hand, are ideal for CARS imaging as their spectral width closely matches the Raman line width. They provide high spectral resolution and vibrational contrast by focusing the pulse energy on a single Raman band [21]. Although comparing with femtosecond, picosecond excitation does lead to a reduction of both the TPEF and SFG signals, it also alleviates nonlinear photodamage so that more excitation power can be used. Therefore, it is still

feasible to acquire high-quality TPEF and SFG images. Thus, picosecond excitation provides a good compromise between the need for high peak power for TPEF and SFG, and the spectral selectivity desired for CARS.

We utilize two mode-locked picosecond Ti:sapphire oscillators (Mira 900, Coherent, Inc., or Tsunami, Spectra Physics) for multimodal NLO imaging. The lasers are synchronized (Synchrolock, Coherent, Inc., or Lock-to-Clock, Spectra Physics) and are tunable in the range of 700–900 nm with output power levels around 1 W. This method provides both a simple and robust source for multimodal NLO imaging and has been applied in numerous areas such as imaging of *ex vivo* guinea pig spinal cord [22] and *in vivo* imaging of mouse sciatic nerve [23]. The disadvantages are as follows: first, the use of two separate lasers and the electronics to synchronize them increases the cost of the system. Second, because the two lasers cannot always be perfectly synchronized, there is a pulse-to-pulse timing jitter. Because of this random jitter, the two pulses do not always overlap exactly in time, thereby increasing the signal fluctuation for both SFG and CARS.

An alternative laser source is the recently demonstrated optical parametric oscillator (OPO) system [24]. This system utilizes a mode-locked picosecond Nd:YVO₄ laser to provide the Stokes beam as well as to synchronously pump an OPO that provides the pump beam. The use of an OPO decreases the cost and it is inherently jitter free. Longer output wavelength than Ti:sapphire lasers further helps to increase penetration depth and reduce photodamage [25]. These features allowed video rate NLO imaging of live mouse ear [24]. A major drawback of this system is the low transmission efficiency of longer wavelengths through microscope optics.

B. Photodamage

Ultrashort laser pulses with high peak power are necessary for efficient NLO signal generation, but under the tight focusing typical in microscopy, such pulses can induce photodamage at the sample due to the high laser intensity at the focal center [26]. In our CARS imaging experiments on tissues, we observed shockwaves and cavitation that agree with the phenomenon of photodisruption induced by plasma generation [27]. The study of the power law between photodamage rate and peak laser power suggested that both linear and second-order nonlinear processes contributed to the damage [22], [28]. Besides linear and two-photon electronic absorption [29] of the laser pulses, we found that Raman-enhanced absorption was another second-order mechanism that can contribute significantly to the photodamage in CARS microscopy [22], [28]. The best laser parameters to suppress photodamage and maintain good signal level depend on the power laws of photodamage rate and signal generation in the experiment.

One way to reduce photodamage is to decrease the pulse peak power. Although NLO signals will be lowered as well, Wang *et al.* showed that two 5-ps lasers of 80 MHz each could generate strong TPEF from elastin and SFG from collagen in pig iliac artery using only 60 mW at the sample with no observed photodamage [30]. This method is the best when the photodamage

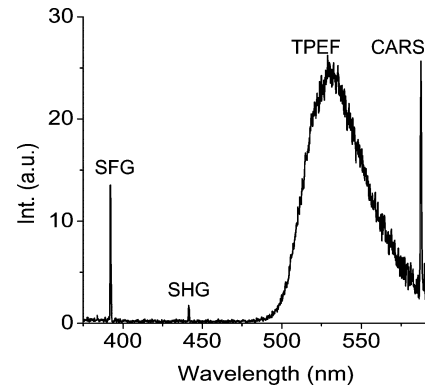


Fig. 3. NLO spectrum of an astrocyte process labeled with Oregon Green BAPTA-2 AM, obtained by using two excitation beams at 705 and 882 nm. Spectrum of SHG peaked at 441 nm, SFG peaked at 392 nm, TPEF band of Oregon Green centered at 530 nm, and CARS peaked at 587 nm. Spectrum acquisition time = 20 ms.

rate has a higher order dependence on laser peak power than signal generation.

When the photodamage rate has a lower order dependence on laser peak power than signal generation, the best method for reducing photodamage is to reduce the repetition rate of the laser pulses [22]. This can be readily accomplished by placing a Pockels' cell in the laser path before the microscope. This method is good for lowering the average power of the excitation beams while still maintaining the high peak power of each pulse. Fu *et al.* demonstrated that reducing the laser repetition rate from 80 to between 1 and 4 MHz with an average power at the sample of only a few milliwatts was an effective means to reduce the photodamage in CARS microscopy as both linear photodamage and two-photon absorption damage processes are of lower order than CARS (third-order process) [22].

C. Signal Detection

Multimodal NLO microscopy is possible because TPEF, SFG, and CARS signals are at different wavelengths that allows for relatively simple separation of signals by dichroic mirrors and appropriate filters. To illustrate this, Fig. 3 shows a spectrum obtained from an astrocyte process labeled with Oregon Green BAPTA-2 AM in guinea pig spinal cord. The pump and Stokes laser beams were focused on the sample with a NA = 1.2 water objective. The diffraction limited focus size is 0.36 μm laterally and 1.3 μm axially. The spectrum was obtained by using the point-scan mode of the microscope to focus the excitation beams on a single astrocyte process and the NLO signals were detected by a spectrometer installed at the back port of our microscope (Fig. 2). For this experiment, the pump and Stokes beams were tuned to 705 and 882 nm, respectively. At the sample, the peak intensity of the pump beam was 2.6 times that of the Stokes beam. A strong SFG signal is seen at 392 nm as well as a weaker SHG peak from the Stokes laser at 441 nm. The SFG peak is more intense because the pump beam had more power and the combined energy of both beams is used for SFG while only one beam is used for SHG. A broad peak from the TPEF of Oregon Green is centered at 530 nm whereas the CARS signal

is located at 587 nm. The spectral separation of these features allowed multimodal NLO imaging of spinal cord white matter isolated from guinea pig [8].

A thoughtful arrangement of detectors is the key to simultaneous TPEF, SFG, and CARS imaging. The forward CARS (F-CARS) signal is highly directional and can be efficiently collected by a $NA = 0.55$ air condenser and directed into a photomultiplier tube (PMT). The backward signal is collected by the same focusing microscope objective. There are three backward PMT detectors in our setup: two internal PMTs (not shown in Fig. 2) inside the scanner box and one external PMT at the back port of the microscope close to the spectrometer in Fig. 2. For the internal PMTs, the signal beam hits a constant point on the detector during laser scanning because it goes through the scanning mirrors. This is called descanned detection. For the external PMT, the signal beam is reflected to the back port by a dichroic mirror in the turret right under the objective. Therefore, the signal beam moves on the detector during scanning. This is called nondescanned detection. A custom-installed dichroic mirror (500 DCXR, Chroma) in the turret reflects any signal shorter than 500 nm to the external PMT. Therefore, the backward SFG signal is externally detected. The backward CARS (epi-, E-CARS) signal and the TPEF signal, longer than 500 nm, will go to the two internal detectors. A 570LP dichroic mirror separates the E-CARS signal and the TPEF signal in 500–570 nm region to be detected separately. This way we can simultaneously detect F-CARS, E-CARS, SFG, and TPEF signals. By switching the dichroic mirror in the turret to 670 DCXR (Chroma), all the signals we are interested in can be reflected to the microscope back port to be detected by the spectrometer or external PMT with proper filters.

PMTs are the preferred detector for multiphoton microscopy. Current GaAsP photocathodes utilized in Hamamatsu H7422 series PMTs provide high quantum efficiency in the range of 400–650 nm but are almost blind to the excitation wavelengths. Although the sensitivity of PMTs is lower than that of avalanche photodiodes (APDs), they are less susceptible to damage by excessive exposure. Furthermore, these detectors have a relatively large active area (~ 5 mm) making them well suited for nondescanned detection at a custom location. It is advantageous to position the detector as close to the sample as possible as signals scattered through tissues can be highly divergent. The low active area of an APD, on the other hand, would possibly lead to reduced field of view in nondescanned detection when the scanning beam moves out of the active area of the APD.

Although PMTs are used in our system, it should be noted that multiple NLO signals can also be simultaneously probed by a high-sensitivity spectrometer. Such scheme allows unmixing of spectrally overlapped signals but needs to be operated at the descanned mode. Alternatively, the CARS and the TPEF signal can also be separated by time-resolved detection.

IV. MULTIMODAL NLO IMAGING OF CENTRAL NERVOUS SYSTEM

The advantages of multimodal NLO microscopy make it a powerful imaging tool for studying complex biological sys-

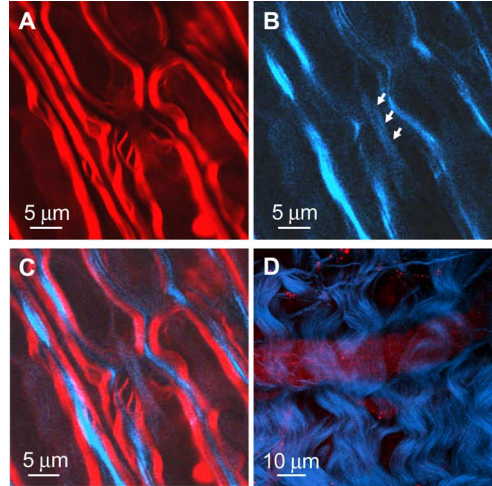


Fig. 4. Multimodal imaging of spinal cord white matter. (A) CARS image of myelin sheath (red). (B) SFG image of astroglial processes (blue) that surround parallel axons and microtubules (blue, indicated by arrows) inside the axon along a node of Ranvier. (C) Overlaid image of (A) and (B). (D) SFG image of astroglial processes (blue) that surround a blood vessel seen with CARS (red). $\omega_p - \omega_s = 2840 \text{ cm}^{-1}$ for each image.

tems such as the central nervous system. Multimodal NLO microscopy can be used to map the organization of different structures such as axonal myelin, astrocyte processes, and microtubules in the central nervous system. The myelin sheath is a multilayered membrane that surrounds the axon of neuron cells and facilitates high-speed impulse conduction. The astrocyte processes interact with neurons to provide structural and trophic support. These two structures in the central nervous system can be readily visualized by CARS and SFG, respectively, as shown in Fig. 4(A–C). Parallel myelin sheath (red, CARS) that wraps the axons is surrounded by astrocyte processes (blue, SFG). The microtubule filaments inside the axon are also clearly visualized. In addition to these structures, the endothelial cell membranes of the blood vessel give a visible CARS contrast. Thus, in a perivascular area, we observed a blood vessel [red in Fig. 4(D)] surrounded by densely packed astrocyte processes [blue in Fig. 4(D)] in the spinal cord.

Multimodal NLO microscopy can also be used to investigate the pathological pathways of neurological diseases. A variety of neurological diseases target the myelin sheath resulting in its damage or loss (i.e., demyelination) [31]. The development of demyelinating lesions is the hallmark of multiple sclerosis, a terminal disease affecting at least 350 000 people in the United States alone [32]. Although multiple sclerosis has been extensively studied for decades, the etiology of this disease remains unclear. Recently, CARS microscopy was applied to follow lysophosphatidyl choline (Lyso-PtdCho) induced myelin degradation in real time [33]. By combining CARS with TPEF, we were able to monitor the Ca^{2+} distribution in healthy and demyelinating states, where the CARS signal from myelin sheath defined the border between intra- and extra-axonal spaces. Fig. 5 shows CARS (red) and TPEF (green) imaging of live spinal tissue before [Fig. 5(A)] and after [Fig. 5(B)] 1 h incubation with Lyso-PtdCho. Extensive and acute myelin swelling [red in

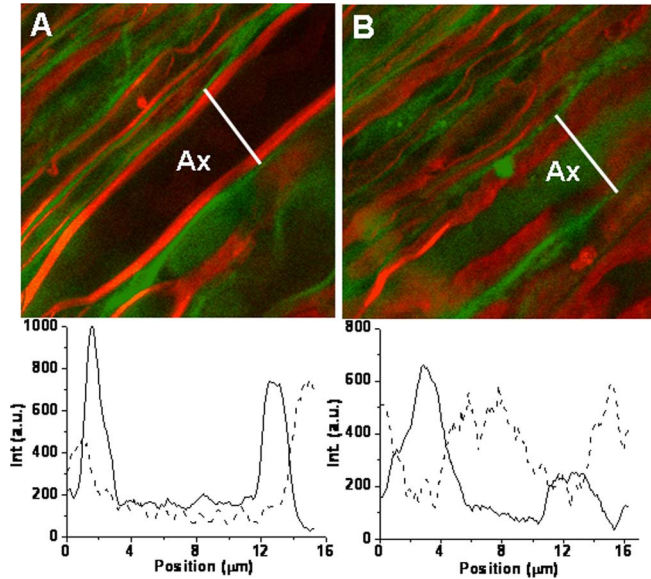


Fig. 5. Simultaneous F-CARS imaging of axonal myelin (red) and TPEF imaging of Ca^{2+} indicator (green) reveals influx of calcium ions into axons during myelin degradation induced by Lyso-PtdCho. (A) 0 min. (B) 61 min after treating the spinal cord white matter with 1% Lyso-PtdCho. Intensity traces along the line indicated are below each image. Solid trace: CARS intensity, dashed trace: TPEF intensity. $\omega_p - \omega_s = 2840 \text{ cm}^{-1}$ for each image. Ax: axon.

Fig. 5(B)] characterized by decrease in CARS signal [see the intensity profile in Fig. 5(B)] was observed. Following treatment with Lyso-PtdCho, the Ca^{2+} concentration in the axons was significantly increased, as seen from the images [Fig. 5(A and B)] as well as the intensity profiles of Oregon Green BAPTA-2. Thus, multimodal NLO imaging demonstrates that Lyso-PtdCho not only induces myelin swelling but also causes Ca^{2+} influx into the axons.

V. CONCLUSION

We have demonstrated multimodal NLO imaging and addressed the considerations in constructing a multimodal NLO microscope. Multimodality is made possible because two synchronized ultrafast lasers can generate CARS, SFG, and TPEF signals at different wavelengths allowing multichannel detection. By utilizing the strengths of each NLO imaging modality to observe different structures, a more complete vision of biological samples can be provided. Furthermore, multimodal NLO microscopy provides real-time noninvasive imaging capability in a laser scanning microscope. These advantages allow multimodal NLO microscopy to be instrumental in addressing biological questions that would otherwise be difficult with other imaging methods.

ACKNOWLEDGMENT

The authors gratefully acknowledge Prof. R. Shi for providing the spinal tissue samples and H.-W. Wang for providing a diagram of the multimodal NLO microscope.

REFERENCES

- [1] P. Morell and R. H. Quarles, "Myelin formation, structure, and biochemistry," in *Basic Neurochemistry: Molecular, Cellular, and Medical Aspects*, G. J. Siegel, B. W. Agranoff, R. W. Albers, and P. B. Molinoff, Eds., 5th ed. Philadelphia, PA: Lippincott Williams & Wilkins, 1999.
- [2] J. H. Simon, "Pathology of multiple sclerosis as revealed by *in vivo* magnetic resonance-based approaches," in *Multiple Sclerosis: Immunology, Pathology, and Pathophysiology*, R. M. Herndon, Ed. New York: Demos, 2003.
- [3] N. Stence, M. Waite, and M. E. Dailey, "Dynamics of microglial activation: A confocal time-lapse analysis in hippocampal slices," *Glia*, vol. 33, pp. 256–266, 2001.
- [4] W. R. Zipfel, R. M. Williams, and W. W. Webb, "Nonlinear magic: Multiphoton microscopy in the biosciences," *Nat. Biotechnol.*, vol. 21, pp. 1369–1377, 2003.
- [5] T. Misgeld and M. Kerschensteiner, "In vivo imaging of the diseased nervous system," *Nat. Rev. Neurosci.*, vol. 6, pp. 449–463, 2006.
- [6] F. Helmchen and W. Denk, "New developments in multiphoton microscopy," *Curr. Opin. Neurobiol.*, vol. 12, pp. 593–601, 2002.
- [7] K. Svoboda and S. M. Block, "Biological applications of optical forces," *Annu. Rev. Biophys. Biomol. Struct.*, vol. 23, pp. 247–285, 1994.
- [8] Y. Fu, H. Wang, R. Shi, and J. X. Cheng, "Second harmonic and sum frequency generation imaging of fibrous astroglial filaments in ex vivo spinal tissues," *Biophys. J.*, vol. 92, pp. 3251–3259, 2007.
- [9] X. Nan, E. O. Potma, and X. S. Xie, "Nonperturbative chemical imaging of organelle transport in living cells with coherent anti-Stokes Raman scattering microscopy," *Biophys. J.*, vol. 91, pp. 728–735, 2006.
- [10] T. T. Le, C. W. Rehrer, T. B. Huff, M. B. Nichols, I. G. Camarillo, and J. X. Cheng, "Nonlinear optical imaging to evaluate the impact of obesity on mammary gland and tumor stroma," *Mol. Imaging*, vol. 6, pp. 205–211, 2007.
- [11] T. T. Le, I. M. Langohr, M. J. Locker, M. Sturek, and J. X. Cheng, "Label-free molecular imaging of atherosclerotic lesions using multimodal nonlinear optical microscopy," *J. Biomed. Opt.*, vol. 12, pp. 054007-1–054007-10, 2007.
- [12] F. Helmchen and W. Denk, "Deep tissue two-photon microscopy," *Nat. Methods*, vol. 2, pp. 932–940, 2005.
- [13] R. W. Boyd, *Nonlinear Optics*. New York: Academic, 2003.
- [14] P. J. Campagnola and L. M. Loew, "Second-harmonic imaging microscopy for visualizing biomolecular arrays in cells, tissues, and organisms," *Nat. Biotechnol.*, vol. 11, pp. 1356–1360, 2003.
- [15] E. Brown, T. Mckee, E. Ditomaso, A. Pluen, B. Seed, Y. Boucher, and R. K. Jain, "Dynamic imaging of collagen and its modulation in tumors *in vivo* using second-harmonic generation," *Nat. Med.*, vol. 9, pp. 796–800, 2003.
- [16] J. X. Cheng and X. S. Xie, "Coherent anti-Stokes Raman scattering microscopy: Instrumentation, theory, and applications," *J. Phys. Chem. B*, vol. 108, pp. 827–840, 2004.
- [17] J. X. Cheng, "Coherent anti-Stokes Raman scattering microscopy," *Appl. Spectrosc.*, vol. 61, pp. 197A–208A, 2007.
- [18] H. Wang, Y. Fu, P. Zickmund, R. Shi, and J. X. Cheng, "Coherent anti-Stokes Raman scattering imaging of axonal myelin in live spinal tissue," *Biophys. J.*, vol. 89, pp. 581–591, 2005.
- [19] K. W. Dunn, R. M. Sandoval, K. J. Kelley, P. C. Dagher, G. A. Tanner, S. J. Atkinson, R. L. Bacallao, and B. A. Molitoris, "Functional studies of the kidney of living animals using multicolor two-photon microscopy," *Amer. J. Physiol. Cell Physiol.*, vol. 283, pp. C905–C916, 2002.
- [20] J. X. Cheng, A. Volkmer, L. D. Book, and X. S. Xie, "An epi-detected coherent anti-Stokes Raman scattering (E-CARS) microscope with high spectral resolution and high sensitivity," *J. Phys. Chem. B*, vol. 105, pp. 1277–1280, 2001.
- [21] E. O. Potma, D. J. Jones, J. X. Cheng, X. S. Xie, and J. Ye, "High-sensitivity coherent anti-Stokes Raman scattering microscopy with two tightly synchronized picosecond lasers," *Opt. Lett.*, vol. 27, pp. 1168–1170, 2002.
- [22] Y. Fu, H. Wang, R. Shi, and J. X. Cheng, "Characterization of photodamage in coherent anti-Stokes Raman scattering microscopy," *Opt. Exp.*, vol. 14, pp. 3942–3951, 2006.
- [23] T. B. Huff and J. X. Cheng, "In vivo coherent anti-Stokes Raman scattering imaging of sciatic nerve tissue," *J. Microsc.*, vol. 225, pp. 175–182, 2007.
- [24] C. L. Evans, E. O. Potma, M. Puoris'haag, D. Côte, C. P. Lin, and X. S. Xie, "Chemical imaging of tissue *in vivo* with video-rate coherent anti-Stokes Raman scattering microscopy," *Proc. Natl. Acad. Sci. USA*, vol. 102, pp. 16807–16812, 2005.

- [25] F. Ganikhanov, S. Carrasco, X. S. Xie, M. Katz, W. Seitz, and D. Kopf, "Broadly tunable dual-wavelength light source for coherent anti-Stokes Raman scattering microscopy," *Opt. Lett.*, vol. 31, pp. 1292–1294, 2006.
- [26] A. Vogel, J. Noack, G. Huettmann, and G. Paltauf, "Femtosecond-laser-produced low-density plasmas in transparent biological media: A tool for the creation of chemical, thermal, and thermomechanical effects below the optical breakdown threshold," *Proc. SPIE*, vol. 46633A, pp. 1–15, 2002.
- [27] P. N. Prasad, *Introduction to Biophotonics*. Hoboken, NJ: Wiley, 2003, pp. 168–175.
- [28] H. Wang, Y. Fu, and J. X. Cheng, "Experimental observation and theoretical analysis of Raman resonance-enhanced photodamage in coherent anti-Stokes Raman scattering microscopy," *J. Opt. Soc. Amer. B*, vol. 24, pp. 544–552, 2007.
- [29] H. J. Koester, D. Baur, R. Uhl, and S. W. Hell, "Ca²⁺ fluorescence imaging with pico- and femtosecond two-photon excitation: Signal and photodamage," *Biophys. J.*, vol. 77, pp. 2226–2236, 1999.
- [30] H.-W. Wang, T. T. Le, and J. X. Cheng, "Label-free imaging of arterial cells and extracellular matrix using a multimodal CARS microscope," *Opt. Commun.*, 2007, doi:10.1016/j.optcom.200.07.067
- [31] R. A. Lazarini, *Myelin Biology and Disorders*, vol. 1. San Diego, CA: Elsevier/Academic, 2004.
- [32] D. W. Anderson, J. H. Ellenberg, C. M. Leventhal, S. C. Reingold, M. Rodriguez, and D. H. Silberberg, "Revised estimate of the prevalence of multiple sclerosis in the United States," *Ann. Neurol.*, vol. 31, pp. 333–336, 1992.
- [33] Y. Fu, H. Wang, T. B. Huff, R. Shi, and J. X. Cheng, "Coherent anti-Stokes Raman scattering imaging of myelin degradation reveals a calcium-dependent pathway in Lyso-PtdCho-induced demyelination," *J. Neurosci. Res.*, vol. 85, pp. 2870–2881, 2007.

Terry B. Huff received the B.S. degree in chemistry from the University of Central Oklahoma, Edmond, in 2004. He is currently working toward the Ph.D. degree in the Department of Chemistry, Purdue University, West Lafayette, IN.

Yunzhou Shi (S'07) received the B.S. degree in electronics science and technology from the University of Science and Technology of China, Hefei, China, in 2005. She is currently working toward the Ph.D. degree at Weldon School of Biomedical Engineering, Purdue University, West Lafayette, IN.

Yan Fu received the B.S. and M.S. degrees in chemistry from Tsinghua University, Beijing, China, in 2000 and 2003, respectively. She is currently working toward the Ph.D. degree at Weldon School of Biomedical Engineering, Purdue University, West Lafayette, IN.

Haifeng Wang (M'01) received the B.S. degree from the Department of Electronic Engineering of Tsinghua University, Beijing, China, in 1998, and the Ph.D. degree from the School of Electrical and Computer Engineering, Purdue University, West Lafayette, IN, in 2003.

Since 2004, he has been a Postdoctoral Fellow at Weldon School of Biomedical Engineering, Purdue University.

Ji-Xin Cheng received the Ph.D. degree in chemistry from the University of Science and Technology of China, Hefei, China, in 1998.

He was a Postdoctoral Fellow at Hong Kong University of Science and Technology and Harvard University. In 2003, he joined Weldon School of Biomedical Engineering, Purdue University, West Lafayette, IN. His current research interests include cell biophysics, nonlinear optical imaging, and nanomedicine development.